Influence of low-temperature chemistry on steady detonations with curvature losses

F. Veiga-López[a,b,*], Z. F. Weng[c], R. Mével[c], J. Melguizo-Gavilanes[a]

[a] *Institut Pprime, UPR 3346 CNRS, ISAE–ENSMA, BP 40109, 86961 Futuroscope–Chasseneuil Cedex, France*
[b] *Fluid Mechanics Research Group, Universidad Carlos III de Madrid, Av. de la Universidad 30, 28911, Leganés (Madrid), España*
[c] *Center for Combustion Energy, School of Vehicle and Mobility, State Key Laboratory for Automotive Safety and Energy, Tsinghua University, 30 Shuang Qing road, 100084 Beijing, China*

November 9, 2022

Abstract

The influence of low temperature chemistry (LTC) on the locus of steady solutions predicted by a ZND model with curvature losses and detailed kinetics was assessed using undiluted / CO_2-diluted stoichiometric DME-O_2 mixtures. Results show (i) the existence of an additional critical point at large velocity deficits when the LTC sub-mechanism is included in the reaction model, and (ii) a shift in the criticality from small to large velocity deficits as CO_2-dilution is increased. Detailed thermo-chemical analyses revealed the importance of LTC in enabling an increased resistance to losses at large velocity deficits. LTC results in a temperature increase of $\sim$ 200 K at the beginning of the reaction zone that activates the intermediate and high temperature reactions, thereafter leading to the main heat release stage. Without a process that replenishes the OH radical pool at postshock temperatures below 1000 K the critical point at large velocity deficits ceases to exist.

Keywords: DME; Detonation modeling; Low temperature chemistry; $D - \kappa$ curves; Curvature losses

1. Introduction

Dimethyl ether (DME, CH_3OCH_3) arises as an alternative to replace conventional non-renewable polluting fuel (e.g., diesel) for transport and industrial applications [1, 2]. Among the advantages of DME are (i) its low-soot emission, (ii) its extended lean-burning efficiency, and (iii) its production potential from a variety of sources (e.g., biomass, natural gas), whereas its most notable drawback is its low energy density since DME is gaseous at ambient conditions; an issue shared with hydrogen and natural gas for mobile applications.

Like any other fuel, the production and handling of DME poses safety hazards. The fact that DME is an oxygenated fuel and that for practical applications requires compression (0.5 MPa), accidental leaks are more likely to lie within the flammable envelope (i.e., 3.5%-19% vol. in air at ambient conditions) [3]; DME is also one of the smallest hydrocarbons to exhibit low temperature chemistry (LTC). Such leaks typically occur in confined environments where, upon ignition, initially harmless flames may accelerate and transition to detonation [4, 5]; a destructive combustion mode that may cause severe structural damage. Besides the above mentioned safety concerns, harnessing the high rates of heat release present in detonations has piqued the interest of scientist and engineers for decades [6, 7]; DME could prove to be a useful fuel for pulse/rotating detonation engines.

Detonation fronts are observed to be curved during their initiation, propagation and diffraction. A successful (low-order) physical model to predict limiting behaviors should most certainly include curvature effects. Extensions to the ZND model including curvature losses yield the locus of steady-state solutions in detonation velocity (D) - curvature (κ) space; the so-called $D-\kappa$ curves. The existence of a maximum curvature, κ_{crit}, in these curves is a sign that this type of low-order models may provide meaningful estimates for detonability limits. Indeed these tools have been used extensively in theoretical studies [8–11] and have shown to be in agreement with experimental data [12–14]. To the best of our knowledge, the influence of LTC on $D-\kappa$ curves has not been assessed. As will be shown, LTC induces non-trivial changes to κ_{crit}, and depending on the conditions considered, may even shift the criticality to large velocity deficits; an outcome that warrants an in-depth investigation of its underlying causes.

Previous work examining LTC effects on deflagration-to-detonation-transition (DDT) and detonations is rather scarce. It ranges from significant reductions in DDT run-up distances (up to 50%) due to faster shock amplification in hydrocarbon-O_2 mixtures [15–18] and easier detonation onset behind incident waves or hot spots in non-diluted / CO_2-diluted mixtures (*n*-hexane / DME) [19–21] to smaller detonation cell widths [22]. In all these studies, LTC occured within the fresh mixture or was activated during the DDT process. In [23] it was shown that adding large amounts of CO_2 to *n*-heptane-O_2 activated LTC at the von Neumann state for Chapman-Jouguet detonations but the length scales associated to the structure are inordinately large to permit experimental observation; the addition of oxygen atoms or hydroxyl radicals precursors to DME-O_2, such as ozone or hydrogen peroxide [24–26], showed significant reductions in the aforementioned lengths which could enable observation at laboratory scale.

The present study supplements those listed above by characterizing the effect of LTC on $D-\kappa$ curves. Undiluted and CO_2-diluted DME-O_2 mixtures are considered. The focus is placed on the characterization of the chemical structure of quasi-steady detonations that propagate at sub-Chapman-Jouguet velocities due to curvature losses. Although it is acknowledged that the assumptions made in deriving the 1-D model neglect some features present in real detonations, such as local unsteadiness and multidimensional effects (i.e., the cellular structure), it provides valuable information about their chemical structure and lends itself to carry out detailed thermo-chemical analyses that properly account for the expected thermodynamic changes in the reaction zone.

2. Formulation

The flow is described by the steady reactive Euler equations including a curvature term, α.

$$\frac{\mathrm{d}\rho}{\mathrm{d}x} = -\frac{\rho}{w}\frac{(\dot{\sigma} - w(1-\eta)\alpha)}{\eta}, \tag{1}$$

$$\frac{\mathrm{d}w}{\mathrm{d}x} = \frac{(\dot{\sigma} - w\alpha)}{\eta}, \tag{2}$$

$$\frac{\mathrm{d}p}{\mathrm{d}x} = -\rho w\frac{(\dot{\sigma} - w\alpha)}{\eta}, \tag{3}$$

$$\frac{\mathrm{d}Y_k}{\mathrm{d}x} = \frac{W_k\dot{\omega}_k}{\rho w} \quad (k = 1, ..., N), \tag{4}$$

where ρ, w, p, and t are the mixture density, axial velocity in the wave-attached frame, pressure, and time, respectively. The mass fraction, molecular weight and net production/consumption rate per unit mass of species k are given by Y_k, W_k and $\dot{\omega}_k$. Here $\eta = 1 - M^2$ is the sonic parameter and $M = w/a_f$ is the Mach number relative to the leading shock computed using the frozen speed of sound, a_f. $\dot{\sigma}$ is the thermicity and $\alpha = 1/A \ \mathrm{d}A/\mathrm{d}x = \kappa\,(D/w - 1)$ the axial area change [9]. The curvature κ is given by $\kappa = 2/R_c$ for spherical waves, and $1/R_c$ for cylindrical waves with R_c being the local radius of curvature. The model is derived under the assumption of weak curvature and quasi-steady propagation. Furthermore, the reactive mixture is assumed to behave as an ideal gas. See supplementary material and [9] for additional details. The implementation in the Shock and

Detonation Toolbox (SDT) [27] only entails adding the terms containing α; the code is available upon request. Two reduced chemical mechanisms for DME are used [28]. Both have 39 species and share 154 reactions but one of them includes 21 extra reactions to account for LTC (R155-R175). These chemical mechanisms were derived from the detailed reaction model of Zhao et al. [29], which contains 55 species and 290 reactions. The mechanism of Zhao et al. has been extensively validated over a wide range of conditions; the experimental data were obtained under both pyrolysis and oxidation, and cover the range of pressure from 4 kPa to 4 MPa; the initial temperature reported for some shock tube experiments was as high as 1600 K. The experimental data include species profiles obtained in a flow reactor, a jet-stirred reactor, and burner-stabilized flames, shock tube ignition delay-time and laminar flame speeds. While the model employed here was reduced to study atmospheric turbulent jet flames, it is important to note that the predictions of the reduced model are almost identical to those of the original model over the range of pressure $p = 0.1 - 3$ MPa and for equivalence ratios $\phi = 0.3 - 2$. These comparisons were performed for ignition delay-time (the metric of interest in the current study), laminar flame speed, and temperature profiles in a perfectly-stirred reactor, and are available in the supplementary material of Bhagatwala et al. [28]. To further verify the trends observed when using the reduced model of Bhagatwala et al. were not induced by the reaction model reduction, additional calculations were performed using the detailed model of Zhao et al. [29]. The same qualitative trends were obtained for the $D-\kappa$ curves, namely, two turning points. The latter located at very similar velocity deficits (D/D_{CJ}), and exhibiting only modest differences in the predicted values of κ. This comparison is shown in the supplementary material of this work. It is also noted that the mechanism of Zhao et al., or its reductions, have previously been used to study detonation in DME-O_2 mixtures; see Ng et al. [30] and Mevel and Gallier [31]. All the above referenced mechanisms are provided in Cantera [32] format (*.cti*) as supplementary material.

3. Results and Discussion

3.1. $D - \kappa$ curves

Figure 1-(a) shows the $D - \kappa$ curves for a stoichiometric DME-O_2 mixture at $p_0 = 100$ kPa and $T_0 = 300$ K. In the upper branch of the curve ($D/D_{CJ} > 0.7$), both detailed mechanisms yield identical results, an upper critical point (UCP) at $D(\kappa_{\text{crit}})/D_{CJ} = 0.93$ with $\kappa_{\text{crit}} = 101.32$ m^{-1}, comparable to that obtained with a stoichiometric H_2-O_2 mixture ($\kappa_{\text{crit}} \sim 160$ m^{-1}) at the same initial conditions. However, in the lower part of the curve ($D/D_{CJ} < 0.7$), differences exist. Without LTC in the chemical mechanism, only a single turning point is obtained, and $\kappa \to 0$ m^{-1} as $D/D_{CJ} \to 0.7$. Including LTC in the chemical mechanism changes the outcome. Two additional turning points appear at $D/D_{CJ} \sim 0.63$ and $D/D_{CJ} \sim 0.58$, respectively. The critical curvature around the lower critical point (LCP) is close to 4 m^{-1}. While this value is much smaller than the UCP it is similar to those obtained with moderately-diluted stoichiometric H_2-air-Ar ($X_{\text{Ar}} > 60\%$) or slightly-diluted H_2-air-N_2 ($X_{\text{N}_2} > 20\%$) blends.

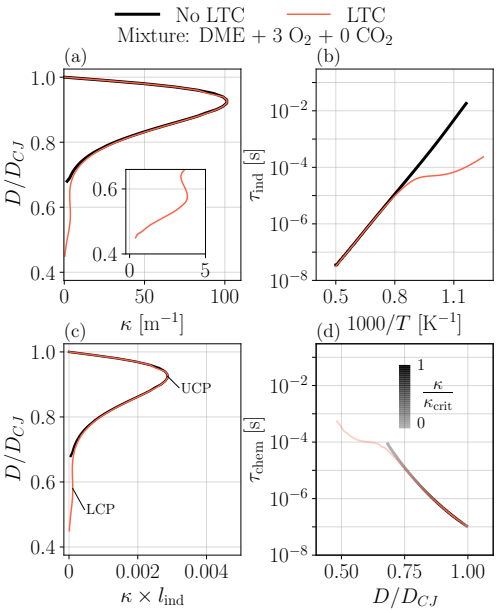

Fig. 1: (a) $D - \kappa$ curves, (b) constant volume induction times, τ_{ind}, at $\rho_{vN} = 16.192$ kg/m^3 (c) $D - \kappa$ curves normalized by l_{ind}, and (d) chemical times, τ_{chem}. Conditions: DME + 3O_2 + 0CO_2 at $p_0 = 100$ kPa and $T_0 = 300$ K.

The difference in behavior may naively be explained by the discrepancies induced by LTC in the delay times at postshock conditions representative of large velocity deficits. In this manuscript, we differentiate between the standard constant volume delay times, τ_{ind}, and the chemical times, τ_{chem}, computed from the integration of the system shown in sec. 2 for a given wave velocity D/D_{CJ}; both are measured to the peak of maximum thermicity. These are shown in Figs. 1-(b) and (d), respectively. The lines in the τ_{chem} plot are shaded by κ_{crit} at UCP; light regions represent D/D_{CJ} away from κ_{crit}. The plots show the delay time reduction typical of LTC for postshock temperature $T_s < 1100$ K while for $T_s > 1250$ K no LTC effects are observed.

As LTC shows a non-negligible influence on the $D - \kappa$ curves, following [25, 26] up to 6 moles of CO_2 were added to stoichiometric DME-O_2 to promote LTC effects while keeping the length scales

Table 1: Velocity, curvature values (D/D_{CJ} , κ [m^{-1}]) at UCP and LCP for DME + $3O_2$ + XCO_2; X denotes the number of moles. The ideal detonation velocity, D_{CJ} [m/s], and induction length, l_{ind} [mm], are also shown.

	$0CO_2$	$2CO_2$	$4CO_2$	$6CO_2$
UCP	(0.93, 101.32)	(0.94, 7.66)	(0.94, 1.21)	(0.94, 0.30)
LCP	(0.58, 3.81)	(0.64, 1.69)	(0.68, 0.89)	(0.71, 0.50)
D_{CJ}	2318.7	1900.9	1690.2	1556.3
l_{ind}	0.028	0.346	2.192	9.208

associated to their spatial structures within reasonable bounds, i.e., $\mathcal{O}$(cm). CO_2 addition reduces the shock strength which results in lower thermodynamics jumps (i.e., postshock conditions) and longer τ_{ind} and τ_{chem}. See Figs. 2-(b) and (d), respectively, obtained for 6 moles of CO_2; key results for intermediate dilutions are summarized in table 1 for completeness.

Even at small velocity deficits LTC effects are evident. The curves start diverging for $D/D_{CJ} < 0.95$, resulting in discrepancies of around 14% in the UCP found at $D/D_{CJ} \sim 0.94$. Only the mechanism with LTC admits solutions for $D/D_{CJ} < 0.77$. Interestingly, LCP ($\kappa_{\text{crit}} = 0.5$ m^{-1}) is greater than UCP ($\kappa_{\text{crit}} = 0.3$ m^{-1}). This finding, while unexpected, confirms the role of LTC in enabling the existence of steady solutions at low velocities that are more resistant to curvature-induced losses than their high velocity counterparts. However, the κ values associated to these solutions (effectively planar waves) raise questions about whether these waves could be realized in practice. The fact that a LCP is also present in undiluted mixtures with κ values comparable to those obtained with H_2-air-diluent mixtures suggest that these may be good test beds to study detonation re-initiation mechanisms driven by LTC.

Next, detailed thermo-chemical analyses are performed to unveil the chemical pathways responsible for the change in behavior discussed above.

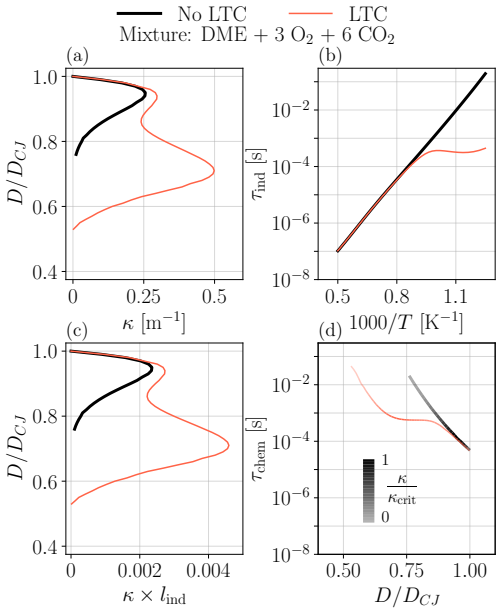

Fig. 2: (a) $D-\kappa$ curves, (b) constant volume induction times, τ_{ind}, at $\rho_{vN} = 14.133$ kg/m^3 (c) $D-\kappa$ curves normalized by l_{ind}, and (d) chemical times, τ_{chem}. Conditions: DME + $3O_2$ + $6CO_2$ at $p_0 = 100$ kPa and $T_0 = 300$ K.

3.2. Thermo-chemical analysis

To better understand the changes induced by LTC on the $D-\kappa$ curves computed, temperature (T/T_0), thermicity ($\dot{\sigma}$) and rate of production ($\text{RoP}_i = \sum_j \left(v''_{i,j} - v'_{i,j}\right) \dot{r}_j$) time histories, as well as the heat release rate ($\text{HRR}_j = \Delta H_j \cdot \dot{r}_j$), and the sensitivity coefficient on temperature ($S_j = k_j/T\, \partial T/\partial k_j$) are examined. In the definitions above, $v''_{i,j}$ and $v'_{i,j}$ are the coefficients of the i^{th} product and reactant in the j^{th} reaction; $\dot{r}_j$ and k_j are the net reaction rate and reaction rate constant of the j^{th} reaction, respectively; ΔH_j is the enthalpy change during the j^{th} reaction. The sensitivity coefficients were calculated by perturbing each reaction rate constant by 1%.

Figure 3 shows T/T_0 and $\dot{\sigma}$ profiles, comparing their behavior for 0 and 6 moles of CO_2 at both UCP (black lines) and LCP (red lines). One, two (or more) peaks are present, denoted by triangular markers, indicating a heat release stage. Unlike UCP, the profile for LCP exhibits significant heat release stages at early times (i.e., $t/\tau_{\text{chem}} \in [0.4, 0.6]$) which may be responsible for shifting the criticality to large velocity deficits; the existence of multiple thermicity peaks in the reaction zone has been previously discussed in the context of steady planar detonations with large CO_2 dilution [25]. The post-shock temperatures at UCP are $T_s = 5.63T_0 = 1688$ K and $T_s = 3.82T_0 = 1145$ K for 0 and 6 moles of CO_2, respectively, thus the heat release is driven by high temperature chemistry (HTC). At LCP, T_s is much lower $3.1T_0 = 927$ K (0 CO_2) and $2.72T_0 = 817$ K (6 CO_2), which correspond to the negative temperature coefficient region shown in Figs. 1(b) and 2(b). At the latter conditions, the HTC pathways are too slow to effectively contribute to the heat release and, consequently, the model does not yield steady so-

lutions at large velocity deficits without LTC (see Figs. 1(a) and 2(a)). Adding the LTC sub-mechanism (R155-R175) to the reaction model activates the first stage of heat release at $T_s < 3.67T_0$ (1100 K), which induces a $\sim 0.67T_0 = 200$ K temperature increase (see inset in Fig. 3(b)), enough to trigger the intermediate and high temperature chemistry that controls the subsequent stages of heat release. For undiluted mixtures, $\dot{\sigma}$ at UCP is much larger than at LCP indicating a strong heat release at UCP, thus yielding larger κ values. A similar argument can be used for highly-diluted mixtures, $\dot{\sigma}$ at LCP is comparable to that at UCP, and during the first stage of heat release, it even surpasses that at UCP potentially explaining the larger κ value obtained at LCP (see Fig. 2(a)).

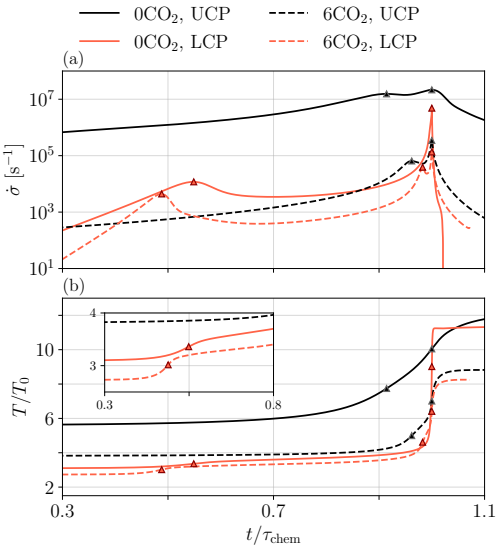

Fig. 3: (a) $\dot{\sigma}$ and (b) T/T_0 profiles at UCP and LCP. Triangular markers denote the thermicity peaks. Conditions: DME + $3O_2$ + XCO_2 at $p_0 = 100$ kPa and $T_0 = 300$ K.

The HRR, RoP and S at each $\dot{\sigma}$ peak provides additional insight. For clarity the $\dot{\sigma}$ peaks will be referred to as $\dot{\sigma}_{P1}$, $\dot{\sigma}_{P2}$ and $\dot{\sigma}_{P3}$ where subscripts P1, P2 and P3 denote the first, second and third stage of heat release. This convention is used throughout this section even for cases in which some of the peaks are not present (see UCP lines for example). As will be shown in the analyses below performed for a mixture with $6CO_2$, these peaks are associated to low, intermediate and high temperature chemistry.

Figure 4 presents the HRR of the four most important reactions at UCP and LCP for $\dot{\sigma}_{P1}$, $\dot{\sigma}_{P2}$ and $\dot{\sigma}_{P3}$. At $\dot{\sigma}_{P1}$ of the LCP, heat is released by O_2 addition (R151), H abstraction (R132) and decomposition (R157) processes; heat is absorbed via isomerization reaction R156. These four reactions are typical of LTC in hydrocarbon fuels [33]. The oxidation of DME starts with R132 through which one H atom is abstracted to generate the CH_3OCH_2 radical. The radical is then oxygenated in R151, and the product isomerizes in R156. This larger molecule finally decomposes in R157 and generates OH radicals which promote R132. Removing the LTC sub-mechanism (R155-R175), although R132 and R151 still take place, the overall reaction cannot proceed without R156 and R157 to continuously produce OH radicals. As a result, LCP does not exist without LTC, as shown in Figs. 1 and 2. At high temperature, the reaction process described above becomes negligible.

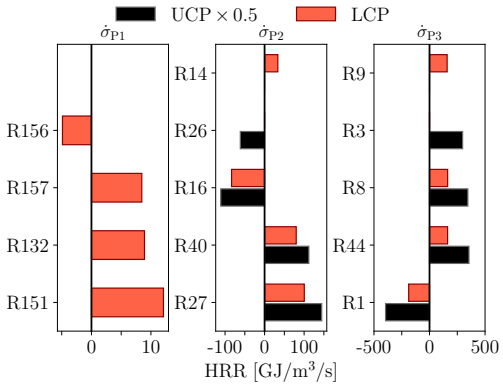

R1: H + O_2 = O + OH
R3: H_2 + OH = H + H_2O
R8: H + OH + M = H_2O + M
R9: H + O_2(+M) = HO_2(+M)
R14: $2HO_2$ = H_2O_2 + O_2
R16: H_2O_2(+M) = 2OH(+M)
R26: HCO + M = CO + H + M
R27: HCO + O_2 = CO + HO_2
R40: CH_2O + OH = H_2O + HCO
R44: CH_3 + O = CH_2O + H
R132: CH_3OCH_3 + OH = CH_3OCH_2 + H_2O
R151: CH_3OCH_2 + O_2 = $CH_3OCH_2O_2$
R156: $CH_3OCH_2O_2$ = $CH_2OCH_2O_2H$
R157: $CH_2OCH_2O_2H$ = $2CH_2O$ + OH

Fig. 4: HRR at the thermicity peaks of the UCP and LCP. Shaded reactions are exclusive to LTC. Conditions: DME + $3O_2$ + $6CO_2$ at $p_0 = 100$ kPa and $T_0 = 300$ K.

The HRR shows that, at $\dot{\sigma}_{P2}$, heat is mostly released by R27 and R40, during which CH_2O is eventually transformed into smaller species, i.e., CO and HO_2. Heat is absorbed by R16 during which this intermediate temperature reaction takes place to generate two OH radicals. OH continues to be the main chain carrier at $\dot{\sigma}_{P2}$. At $\dot{\sigma}_{P3}$, the H radical becomes the main chain carrier, thus the overall reaction is governed by high temperature chemistry (HTC). Heat is absorbed by the chain-branching reaction R1, while the heat release is governed by R3, R8, R44 at UCP and by R8, R9, R44 at LCP. Note that the the HRR at $\dot{\sigma}_{P2}$ and $\dot{\sigma}_{P3}$ is one to two orders of magnitude higher than the values at $\dot{\sigma}_{P1}$, indicating that the former two are the major contributors to the total heat release.

Figure 5 presents the RoP of DME. At UCP DME reacts with CH_3 right after the shock via R134 which indicates that DME readily decomposes into hydrocarbon radicals at high temperature; CH_3 being the most prominent radical blocking the reaction paths of LTC. R132 is negligible at early stages and be-

comes dominant at later time as OH radical is gradually generated through HTC processes. At LCP the post-shock temperature is low which results in slower production of CH_3 radical making the OH radical the key chain carrier. The first stage of heat release is accompanied by a pulse in the RoP of R132.

The HRR and RoP of DME reveal that, while the reactions at UCP and LCP are initiated by different mechanisms, both reach similar reaction paths during the main heat release stage. At LCP, the reaction starts with LTC since the post-shock temperature is low, and the heat released by LTC creates the conditions to trigger HTC. In contrast, the reaction at UCP starts directly through HTC pathways. When the shock speed is low, the detonation wave can only be sustained via LTC pathways.

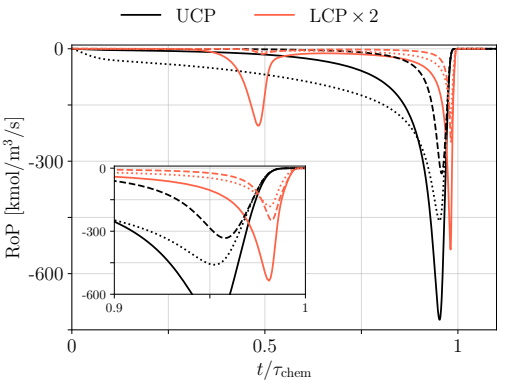

R132: $CH_3OCH_3 + OH = CH_3OCH_2 + H_2O$
R133: $CH_3OCH_3 + H = CH_3OCH_2 + H_2$
R134: $CH_3 + CH_3OCH_3 = CH_3OCH_2 + CH_4$

Fig. 5: DME RoP profiles at UCP and LCP. Conditions: DME + $3O_2$ + $6CO_2$ at $p_0 = 100$ kPa and $T_0 = 300$ K.

The thermo-chemical analyses are further supported by the RoP of the OH radical pool presented in Fig. 6. The OH radical is a key marker of LTC [25, 33, 34]. At $\dot{\sigma}_{P1}$, the OH radical is mainly generated by R157 and R160 and consumed by R40 and R132. Without LTC, R157 and R160 are not active and R40 and R132 cannot proceed; consequently, no steady solutions are possible at low speeds. As the reactions proceed to $\dot{\sigma}_{P2}$ and $\dot{\sigma}_{P3}$, the dominant reactions at UCP and LCP are exactly the same. At $\dot{\sigma}_{P2}$, the OH radical is mostly generated by the intermediate temperature reaction R16 and consumed by R40. At $\dot{\sigma}_{P3}$, the OH radical is produced and consumed by HTC, namely R1-R4. The transition of dominant OH-related reactions from low to intermedaite and high temperature was also discussed in [34] for hot spot ignition in DME/air mixture. However, the underlying mechanisms differ. In their work, a cool flame governed by LTC is first initiated, producing a OH radical barrier as it propagates which attenuates the diffusion

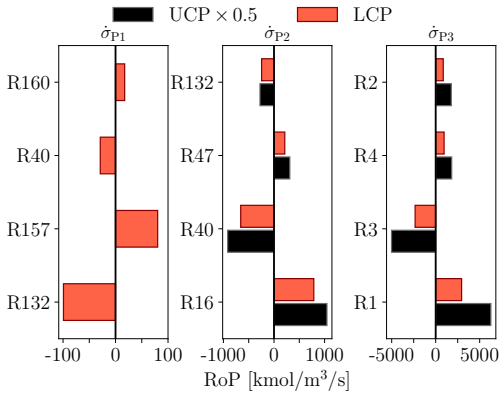

R1: $H + O_2 = O + OH$
R2: $H_2 + O = H + OH$
R3: $H_2 + OH = H + H_2O$
R4: $H_2O + O = 2OH$
R16: $H_2O_2(+M) = 2OH(+M)$
R40: $CH_2O + OH = H_2O + HCO$
R47: $CH_3 + HO_2 = CH_3O + OH$
R132: $CH_3OCH_3 + OH = CH_3OCH_2 + H_2O$
R157: $CH_2OCH_2O_2H = 2CH_2O + OH$
R160: $HO_2CH_2OCHO = OCH_2OCHO + OH$

Fig. 6: OH RoP at the thermicity peaks of the UCP and LCP. Shaded reactions are exclusive to LTC. Conditions: DME + $3O_2$ + $6CO_2$ at $p_0 = 100$ kPa and $T_0 = 300$ K.

of OH radical towards the fresh mixture. This barrier allows a hot flame to establish at later times. The temperature increment induced by the cool flame is of less than 50 K [34]. In our case instead, the LTC induces the first stage of heat release and increases the temperature by $\sim$ 200 K, activating the intermediate and high temperature chemistry to support detonation propagation.

Finally, the sensitivity of temperature to reaction rate constants is presented in Fig. 7. At UCP, the four reactions with higher sensitivity coefficient at $\dot{\sigma}_{P2}$ and $\dot{\sigma}_{P3}$ are the same. The reaction with the highest coefficient is R134, which is the main consumption pathway of DME immediately after shock heating (see Fig. 5). Among the four key reactions at UCP, CH_3 is involved in R43, R48 and R134, which again indicates that CH_3 is one of the markers for HTC. At LCP, the key reactions are essentially similar at the three peaks. Notably, the three most sensitive reactions (R156-R158) all belong to the LTC sub-mechanism (R155-R175). While the analyses of HRR and RoP have shown that LTC mainly take places during the first stage of heat release around $\dot{\sigma}_{P1}$, R156-R158 are still the most sensitive reactions at $\dot{\sigma}_{P2}$ and $\dot{\sigma}_{P3}$. This observation supports the idea that LTC is the essential starting point of the whole reaction process at LCP. However, LTC alone does not release enough heat to drive the propagation (see Fig. 4). The role of LTC is to increase the temperature and create radicals so that the HTC can be triggered. Note that R156-R158 are equally important at each heat release peak which also indicates that the O_2 addition, isomerization and

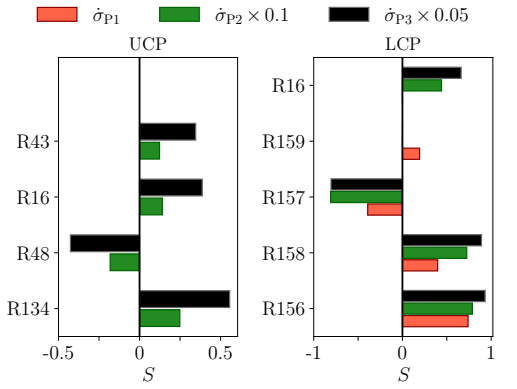

R16: H_2O_2(+M) = 2OH(+M)
R43: $CH_2O + CH_3 = CH_4 + HCO$
R48: $2CH_3$(+M) = C_2H_6(+M)
R134: $CH_3 + CH_3OCH_3 = CH_3OCH_2 + CH_4$
R156: $CH_3OCH_2O_2 = CH_2OCH_2O_2H$
R157: CH2OCH2O2H = $2CH_2O$ + OH
R158: $CH_2OCH_2O_2H + O_2 = O_2CH_2OCH_2O_2H$
R159: $O_2CH_2OCH_2O_2H = HO_2CH_2OCHO$ + OH

Fig. 7: Sensitivity coefficient on temperature at the thermicity peaks of the UCP and LCP. Shaded reactions are exclusive to LTC. Conditions: DME + $3O_2$ + $6CO_2$ at $p_0 = 100$ kPa and $T_0 = 300$ K.

chain-branching processes are all indispensable processes.

3.3. Discussion and potential implications

One important feature of $D - \kappa$ curves is that the rightmost turning point provides the maximum curvature that a steady detonation is able to sustain. For chemical systems without LTC, there is only one turning point which corresponds to the upper turning point (UCP in our study). Experimental and numerical studies on detonation have shown that under certain situations, such as detonation diffraction [35], and detonation propagation in expanding channels with constant area divergence [12, 36], the $D - \kappa$ model predicts closely the velocity deficits for mixtures with low effective activation energy. Likewise, this model has also been shown to reproduce the behavior of near-limit detonations in narrow channels [14]. For all the DME-based mixtures investigated, two critical points exist in the $D - \kappa$ curve. The appearance of a second critical point is due to LTC; notably, the reaction zones in the low speed regime show multiple stages of heat release. Having multiple stages of heat release, however, is not a sufficient condition to obtain a $D - \kappa$ curve with several critical points. For instance, H_2-NO_2/N_2O_4 rich mixtures feature a two-step heat release behavior in the ZND profile [37, 38]; $D - \kappa$ curves computed by us using the same mixture yield one critical point only. This difference in behavior is due to having both stages of heat release fully coupled; there is no switch of dominant chemical pathways and the two stages exist over the full range of conditions described by the $D - \kappa$ curve. Conversely, for DME-based mixtures with LTC, there is a clear switch of the dominant chemical pathways: at high temperature, LTC does not take place whereas at low temperature, LTC is crucial to activate the intermediate and high temperature chemistry.

The results of our study raise new questions and suggest avenues worth exploring in future. The effect of the LCP on detonation propagation in tubes and their transmission to open space is not straightforward to assess; combined experimental and numerical studies are needed to clarify these aspects. The existence of a second critical point in the low velocity regime may result in non-trivial re-initiation dynamics for diffracting detonations, i.e., at very low shock speeds after quenching has occurred past the UCP. Similar outcomes may be hypothesized for detonation propagation in expanding channels; LTC might enable propagation at low speeds in the vicinity of the LCP. Recall that for undiluted DME-O_2 mixtures, the predicted curvature at LCP is comparable to that of typical fuel-air mixtures, ~ 4 m^{-1}, and it becomes quite small, ~ 0.5 m^{-1}, at high CO_2 content. The latter κ values at LCP would result in radii of curvature, $R_c = 1/\kappa = 0.25$ m and 2 m for cylindrical waves (i.e. detonation propagation in diverging/narrow channels), and $R_c = 2/\kappa = 0.5$ m and 4 m for spherical waves (i.e. detonation transmission to open volumes). Clever numerical / experimental studies targeting the states predicted by the steady state theory are needed to provide relevant insight.

Two-dimensional simulations of detonation propagation in marginal channels (i.e., channel heights slightly below the average cell size of the mixture), detonation diffraction and detonation-interaction with inert layers constitute good test cases to verify the leads that the 1D model provides in more realistic settings. Particularly, in light of the cellular structure ubiquitous in multidimensional detonations. The controlled decoupling of the leading shock and reaction zone in such configurations is a key aspect that would in principle result in postshock states for which LTC can be active and influence detonation propagation.

A number of practical implications also come to mind. First, near the detonation limit, galloping behavior is observed with repetitive acceleration-deceleration cycles [39, 40]. The combustion wave propagates at low speeds ($\sim 0.4 D_{CJ}$) for long periods very likely activating LTC which could promote the re-initiation of the wave and potentially modify its intrinsic galloping frequency. Moreover, this LTC-induced behavior might result in an increase of the detonability envelope, similar to what was observed for flammability in [41]. Second, in pulsed detonation engines (PDE), high-repetition rates of the filling-firing cycle are needed to ensure stable thrust. To this end, the use of pre-detonators to guarantee fast

initiation of the detonation wave has been proposed. Typical designs use direct detonation initiation of a highly reactive mixture in a narrow channel to initiate readily a detonation in a less-reactive mixture upon transmission. In [42] several designs of PDE pre-detonators capable of creating toroidal imploding detonation waves were studied. It could be argued that the LTC behavior shown in our results could improve their performance. Finally, LTC could also play a role in detonation initiation in internal combustion engines since the temperature before detonation onset is typically well below 1000 K [43, 44].

4. Conclusion

The influence of LTC on the locus of steady solutions predicted by the $D-\kappa$ model was assessed using undiluted and CO_2-diluted stoichiometric DME-O_2 mixtures. Non-trivial outcomes were found: (i) the existence of a second critical point (LCP) if and only if the LTC submechanism (R155-175) is included in the reaction model; and (ii) a shift in the criticality, κ_{crit}, from small to large velocity deficits as CO_2-dilution is increased (i.e., κ at LCP $>$ κ at UPC). Detailed thermo-chemical analyses revealed the importance of LTC in enabling the increased resistance to curvature-induced losses in the low velocity regime. The production of OH radicals during early stages of heat release as a result of R157 is crucial to activate R132; LTC increases the mixture temperature by $\sim$ 200 K, which enables the intermediate and high temperature reactions take over thereafter leading to the main heat release stage. Without a process that replenishes the OH radical pool at low temperatures (T_s $<$ 1000 K) the LCP ceases to exist. Potential implications of our findings were also discussed.

Acknowledgments

FVL and JMG acknowledge the financial support from the Agence Nationale de la Recherche Program JCJC (FASTD ANR-20-CE05-0011-01). FVL also thanks the travel financial support by the Madrid Government (Comunidad de Madrid-Spain) under the Multiannual Agreement with UC3M in the line of Excellence of University Professors (EPUC3M22).

Supplemental material

Detailed reaction models in Cantera (.cti) format and a complete derivation of the 1D model.

References

[1] S. C. Sorenson, Dimethyl ether in diesel engines: progress and perspectives, J. Eng. Gas Turbines Power 123 (3) (2001) 652–658.

[2] O. I. Awad, X. Ma, M. Kamil, O. M. Ali, Y. Ma, S. Shuai, Overview of polyoxymethylene dimethyl ether additive as an eco-friendly fuel for an internal combustion engine: Current application and environmental impacts, Sci. Total Environ. 715 (2020) 136849.

[3] Y. Kobayashi, S. Nakaya, M. Tsue, Laser-induced spark ignition for DME–air mixtures with low velocity, Proc. Comb. Inst. 37 (3) (2019) 4127–4135.

[4] G. Ciccarelli, S. Dorofeev, Flame acceleration and transition to detonation in ducts, Prog. Energy Combust. Sci 34 (4) (2008) 499–550.

[5] J. E. Shepherd, Detonation in gases, Proc. Comb. Inst. 32 (1) (2009) 83–98.

[6] P. Wolański, Detonative propulsion, Proc. Comb. Inst. 34 (1) (2013) 125–158.

[7] D. P. Stechmann, S. D. Heister, A. J. Harroun, Rotating detonation engine performance model for rocket applications, J. Spacecr. Rockets 56 (3) (2019) 887–898.

[8] R. Klein, Analysis of accelerating detonation using large activation energy asymptotics, Le Journal de Physique IV 5 (C4) (1995) C4–443.

[9] R. Klein, J. Krok, J. Shepherd, Curved quasi-steady detonations. asymptotic analysis and detailed chemical kinetics., Tech. Rep. FM95-04, GALCIT (1995).

[10] J. Yao, D. Stewart, On the normal shock velocity-curvature relationship for materials with large activation energy, Combust. Flame 100 (1995) 519–528.

[11] L. He, P. Clavin, On the direct initiation of gaseous detonations by an energy source, J. Fluid Mech. 277 (1994) 227–248.

[12] M. Radulescu, B. Borzou, Dynamics of detonations with a constant mean flow divergence, J. Fluid Mech. 845 (2018) 346–377.

[13] J. Chao, H. Ng, J. Lee, Detonability limits in thin annular channels, Proc. Comb. Inst. 32 (2) (2009) 2349–2354.

[14] X. Shi, J. Crane, H. Wang, Detonation and its limit in small tubes with ozone sensitization, Proc. Combust. Inst. 38 (2021) 3547–3554.

[15] K. Shchelkin, A. Sokolik, Zh. Fiz. Khim. 10 (1937) 589–596.

[16] M. Romano, M. Radulescu, A. Higgins, J. Lee, Sensitization of pentane-oxygen mixtures to DDT via cool flame oxidation, Combust. Flame 132 (2003) 387–394.

[17] V. Basevich, B. Lidskii, S. Frolov, Mechanisms of the amplification of a shock wave passing through a cool flame zone, Russ. J. Phys. Chem. B 4 (1) (2010) 101–109.

[18] N. Chaumeix, B. Imbert, L. Catoire, C.-E. Paillard, The onset of deonation behind shock waves of moderate intensity in gas phase, Combust. Sci. Technol. 186 (2014) 607–620.

[19] W. Han, J. Huang, W. Liang, C. Wang, R. Mevel, C. Law, Unsteady propagation of detonation with multi-stage heat release, Fuel 296 (2021) # 120666.

[20] P. Dai, Z. Chen, Supersonic reaction front propagation initiated by a hot spot in n-heptane/air mixture with multistage ignition, Combust. Flame 162 (2015) 4183–4193.

[21] P. Dai, Z. Chen, X. Gan, Autoignition and detonation development induced by a hot spot in fuel-lean and CO_2 diluted n-heptane/air mixtures, Combust. Flame 201 (2019) 208–214.

[22] M. Romano, M. Radulescu, A. Higgins, J. Lee, W. Pitz, C. Westbrook, Sensitization of hydrocarbon-oxygen mixtures to detonation via cool-flame oxidation, Proc. Combust. Inst. 29 (2002) 2833–2838.

[23] W. Liang, R. Mével, C. K. Law, Role of

low-temperature chemistry in detonation of n-heptane/oxygen/diluent mixtures, Combust. Flame 193 (2018) 463–470.
[24] R. Mevel, J. Melguizo-Gavilanes, M. Radulescu, Znd structure of cool detonation in dimethyl ether-oxygen-carbon dioxide mixtures, Proc. ASPACC 11 (2017).
[25] Y. He, R. Mével, Effect of hydroxyl radical precursor addition on LTC-affected detonation in DME–O_2–CO_2 mixtures, Shock Waves 30 (7) (2020) 789–798.
[26] R. Mével, Y. He, Effect of oxygen atom precursors addition on LTC-affected detonation in DME–O_2–CO_2 mixtures, Shock Waves 30 (7) (2020) 799–807.
[27] S. Browne, J. Ziegler, J. Shepherd, Numerical solution methods for shock and detonation jump conditions, GALCIT report FM2006 6 (2008) 90.
[28] A. Bhagatwala, Z. Luo, H. Shen, J. A. Sutton, T. Lu, J. H. Chen, Numerical and experimental investigation of turbulent DME jet flames, Proc. Comb. Inst. 35 (2) (2015) 1157–1166.
[29] Z. Zhao, M. Chaos, A. Kazarov, F. Dryer, Thermal decomposition reaction and a comprehensive kinetic model of dimethyl ether, International Journal of Chemical Kinetics 40 (2008) 1–18.
[30] H. Ng, J. Chao, T. Yatsufusa, J. Lee, Measurement and chemical kinetic prediction of detonation sensitivity and cellular structure characteristics in dimethyl ether-oxygen mixtures, Fuel 88 (2009) 124–131.
[31] R. Mevel, S. Gallier, Structure of detonation propagating in lean and rich dimethyl ether-oxygen mixtures, Shock Waves 28 (2018) 955–966.
[32] D. G. Goodwin, R. L. Speth, H. K. Moffat, B. W. Weber, Cantera: An object-oriented software toolkit for chemical kinetics, thermodynamics, and transport processes, version 2.5.1 (2021).
[33] J. Zádor, C. A. Taatjes, R. X. Fernandes, Kinetics of elementary reactions in low-temperature autoignition chemistry, Prog. Energy Combust. Sci. 37 (4) (2011) 371–421.
[34] Y. Wang, H. Zhang, T. Zirwes, F. Zhang, H. Bockhorn, Z. Chen, Ignition of dimethyl ether/air mixtures by hot particles: Impact of low temperature chemical reactions, Proc. Comb. Inst. 38 (2) (2021) 2459–2466.
[35] M. Arienti, J. Shepherd, A numerical study of detonation diffraction, J. Fluid Mech. 529 (2005) 117–146.
[36] Q. Xiao, M. Radulescu, Role of instability on the limits of laterally strained detonation waves, Combust. Flame 220 (2020) 410–428.
[37] F. Joubert, D. Desbordes, H. Presles, Detonation cellular structure in NO_2/N_2O_4-fuel gaseous mixtures, Combust. Flame 152 (2008) 482–495.
[38] D. Davidenko, R. Mével, G. Dupré, Numerical study of the detonation structure in rich H_2-NO_2/N_2O_4 and very lean H_2-N_2O mixtures, Shock Waves 21 (2011) 85–99.
[39] J. H. S. Lee, The Detonation Phenomenon, Cambridge University Press, 2008.
[40] S. Jackson, B. Lee, J. Shepherd, Detonation mode and frequency analysis under high loss conditions for stoichiometric propane-oxygen, Combust. Flame 167 (2016) 24–38.
[41] W. Liang, C. Law, Extended flammability limits of n-heptane/air mixtures with cool flames, Combust. Flame 185 (2017) 75–81.
[42] S. Jackson, Gaseous detonation initiation via wave implosion, Ph.D. thesis, Caltech (2005).
[43] Z. Wang, Y. Qi, H. Liu, P. Zhang, X. He, J. Wang, Shock wave reflection induced detonation (SWRID) under high pressure and temperature condition in closed cylinder, Shock Waves 26 (2016) 687–691.
[44] Y. Wang, S. Xiang, Y. Qi, R. Mével, Z. Wang, Shock wave and flame front induced detonation in rapid compression machine, Shock Waves 28 (2018) 1109–1116.